Kinetic arrest and glass-glass transition in short-ranged attractive colloids

M. Sztucki, T. Narayanan,* G. Belina, and A. Moussaïd
European Synchrotron Radiation Facility, BP 220, 38043 Grenoble, France

F. Pignon
Laboratoire de Rhologie, CNRS, UMR 5520, 38041 Grenoble, France

H. Hoekstra†
Katholieke Universiteit Leuven, W. de Croylaan 46, 3001 Leuven, Belgium
(Received 6 July 2006; published 17 November 2006)

A thermally reversible repulsive hard-sphere to sticky-sphere transition was studied in a model colloidal system over a wide volume fraction range. The static microstructure was obtained from high resolution small angle x-ray scattering, the colloid dynamics was probed by dynamic x-ray and light scattering, and supplementary mechanical properties were derived from bulk rheology. At low concentration, the system shows features of gas-liquid type phase separation. The bulk phase separation is presumably interrupted by a gelation transition at the intermediate volume fraction range. At high volume fractions, fluid-attractive glass and repulsive glass-attractive glass transitions are observed. It is shown that the volume fraction of the particles can be reliably deduced from the absolute scattered intensity. The static structure factor is modeled in terms of an attractive square-well potential, using the leading order series expansion of Percus-Yevick approximation. The ensemble-averaged intermediate scattering function shows different levels of frozen components in the attractive and repulsive glassy states. The observed static and dynamic behavior are consistent with the predictions of a mode-coupling theory and numerical simulations for a square-well attractive system.

DOI: 10.1103/PhysRevE.74.051504 PACS number(s): 64.70.Pf, 82.70.Dd, 61.10.Eq, 82.70.Gg

I. INTRODUCTION

One of the fascinating features of colloidal systems is that they allow us to simulate the simplest interaction potential, namely the hard-sphere potential [1,2]. The well-known example is the sterically stabilized colloidal particles suspended in a good solvent for the stabilizing layer [1]. It has been well established that this simple system can exhibit fluid, crystal, and glassy phases, as well as their coexistence as a function of the volume fraction ϕ analogous to that in atomic systems [2]. Colloidal systems have the advantage that the interparticle potential can be tuned. Moreover, the length and the time scales of the microstructure and the dynamics are more accessible to laboratory experiments. As a result these systems readily permit us to quantitatively verify the predictions of statistical mechanical theories and computer simulations [1,2].

With the introduction of a short-ranged attractive interaction to the repulsive hard-core potential, additional features appear in the phase diagram. The classical example is the Baxter's sticky hard-sphere model [3]. This model potential involves an infinitely deep attraction at close contact (sticky surface). The resulting phase diagram at low ϕ range shows a gas-liquid type phase separation with a critical point [4]. Beyond the critical region, there exists a line of gelation which extends to high ϕ range. While Baxter's model is relatively simple to be studied using Ornstein-Zernike (OZ) integral equation and Percus-Yevick (PY) approximation, it has a rather unphysical infinitely deep potential at close contact [5]. Consequently, the square-well (SW) attraction has been proposed as a more realistic interaction than the Baxter potential to mimic colloidal systems with short-ranged attraction [5,6]. In this case, the potential, $V(r)$, has a finite width Δ and depth u. Recently, such colloidal systems have received considerable renewed interest in terms of their dynamical properties [6–12]. Mode coupling theory (MCT) [6,13] and computer simulations (CS) [14,15] have successfully predicted two different glass transitions (as schematically presented in Fig. 1). In the conventional repulsive colloidal glass, the ergodicity is lost due to blocking of particle diffusion by the dense surrounding cages formed by their nearest neighbors. In the attractive glass, the particle motion is jammed even at low ϕ by the short-ranged attraction or stickiness. The stickiness is characterized by the parameter τ_B which is an effective temperature [5]. These two glass lines meet at high ϕ defining a reentrant transition of repulsive glass-fluid-attractive glass as the attractive interaction is progressively increased for a certain range of Δ [6,13]. The attractive glass line extends beyond the reentrant region to a higher order singular point in MCT (A_3) delineating a glass-glass transition [8]. In experiments, similar dynamical arrest including the reentrant transition [16–18] as that predicted by theory and simulation have been observed in a diverse class of short-ranged attractive colloidal systems [19–24].

This paper presents a detailed investigation of the evolution of static structure and dynamics in a model short-ranged attractive colloidal system. The experimental system consisted of sterically stabilized silica particles in a marginal solvent. In this case, the transition between attractive and

*Electronic address: narayan@esrf.fr
†Present address: DSM Research, P. O. Box 18, 6160 MD Geleen, The Netherlands.

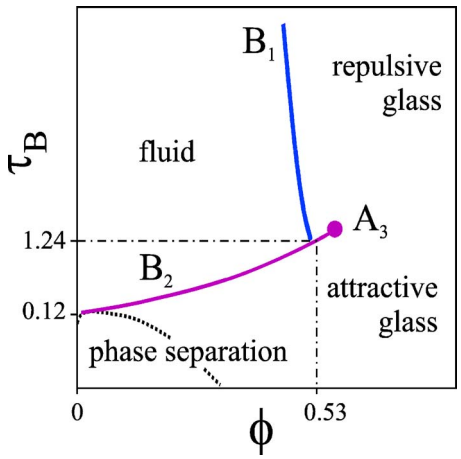

FIG. 1. (Color online) A schematic phase diagram of spherical particles interacting by a square-well potential, illustrating the repulsive (B_1) and attractive (B_2) glass transition lines which meet at high ϕ near the third order singular point A_3 in MCT. At intermediate ϕ, the approach to the phase separation and the associated critical point is interrupted by B_2. The indicated values of ϕ and τ_B are obtained experimentally in this work.

repulsive states is thermally reversible and occurs at a well defined temperature, T_A. As a result the attractive interaction can be turned on and off by a simple variation of temperature. The phase diagram and static microstructure were obtained from quantitative ultra small-angle x-ray scattering (USAXS) experiments. The dynamical behavior was probed by dynamic light scattering and x-ray scattering (DLS and DXS, respectively). These dynamic scattering studies were complemented by bulk rheological measurements allowing us to extract the low-frequency mechanical properties of the system. The present work directly investigated the evolution of SW parameters and the corresponding changes in dynamical behavior at different ϕ ranges. As ϕ is systematically increased, the intermediate range clustering and gelation behavior crossed over to a region of higher order glass transitions. In this higher ϕ region, the static structure factor showed only subtle variations but particle dynamics and bulk rheology changed dramatically with the onset of attraction. From the long time behavior of intermediate scattering function and the frequency dependence of shear moduli, a transition between attractive and repulsive glasses was identified. At still higher $\phi \sim 0.6$, the repulsive-attractive glass transition appears to be characterized by a peculiar dynamical state suggestive of slow propagation and damping of acoustic waves in the sample. In addition, the yielding behavior of attractive glass and the transition to fluidlike behavior were examined.

II. THEORETICAL BACKGROUND

A. Static structure

The scattered intensity $I(q)$ from a colloidal suspension of monodisperse spherical particles can be expressed as follows [25]:

$$I(q) = N_p \Delta\rho^2 V_p^2 P(q) S(q), \tag{1}$$

where N_p is the colloid number density, $\Delta\rho = \rho_p - \rho_m$ is the scattering contrast with ρ_p and ρ_m being the x-ray scattering length densities for the particle and the suspending medium, respectively. V_p is the average particle volume, $P(q)$ is the form factor describing the shape of the particles, and $S(q)$ is the structure factor of interparticle interaction. The scattering vector, $q = (4\pi/\lambda_0)\sin(\theta/2)$, depends on the scattering angle θ and the incident x-ray wave length λ_0.

$P(q)$ can be determined from a dilute noninteracting sample. The measured $P(q)$ for the silica colloidal particles used in this work is adequately described by a polydisperse sphere scattering function with Schulz size distribution. In this case, the polydisperse $P(q)$ $[\langle P(q) \rangle]$ has an analytical expression [26].

The structure factor of a short-ranged interacting colloidal system can be calculated using the OZ integral equation and the PY approximation [27]. The resulting S(q) $[S^{\mathrm{PY}}(q)]$ is related to ϕ and the interparticle potential $V(r)$ through the direct correlation function $C(r)$[27]

$$S(q) = 1/[1 - N_p C(q)], \tag{2}$$

where $C(q)$ is the Fourier transform of $C(r)$. For a hard-sphere system, N_p is related to ϕ as

$$\phi_{HS} = \pi N_p \sigma^3/6 \tag{3}$$

where σ is the effective hard-sphere diameter, which includes not only the diameter of the core but also the nonpenetrable thickness of the shell.

For a short-ranged attractive system the interparticle interaction is approximately described by hard-sphere repulsion with an attractive square-well potential [5,6,28,29]

$$V(r) = \begin{cases} \infty & 0 < r < \sigma \\ -u & \sigma \leqslant r \leqslant \sigma + \Delta \\ 0 & \sigma + \Delta < r \end{cases}, \tag{4}$$

where u and Δ are the depth and the width of the attractive square well, respectively. The strength of attraction is characterized by the stickiness parameter τ_B [5],

$$\tau_B = [1/(12\epsilon)]\exp(-u/k_B T), \tag{5}$$

with

$$\epsilon = \Delta/(\sigma + \Delta). \tag{6}$$

$C(q)$ for a square-well attractive system can be expressed analytically using the leading order series expansion of the PY approximation [5,6,28,29] with the effective volume fraction ϕ_{SW},

$$\phi_{SW} = \pi N_p (\sigma + \Delta)^3/6. \tag{7}$$

The $S(q)$ of the square-well system can also be calculated in the mean spherical approximation (MSA), which assumes a constant $C(r)$ within the well [6,25]. However this solution has a tendency to over-predict the potential well parameters and a suitable rescaling is necessary to compare with the numerical results [6].

The polydispersity of the particles not only influences $P(q)$ but also $S(q)$ [27]. Therefore, the interparticle interaction of a polydisperse system is described by an effective $S(q)$ [$S_M(q)$]. At low and intermediate ϕ, $S_M(q)$ can be calculated using the *decoupling approximation*, which has an analytical expression in the case of a Schulz size distribution [26]. In this approximation, $S_{\mathrm{M}}(q)$ is related to the monodisperse $S(q)$ by the following expression [26,27]:

$$S_{\mathrm{M}}(q) = 1 + \frac{\langle F(q)\rangle^2}{\langle F^2(q)\rangle}[S(q) - 1], \tag{8}$$

where $F(q)$ is the form amplitude with $\langle P(q)\rangle = \langle |F(q)|^2\rangle$. The decoupling approximation has limited applicability and it fails at high ϕ and high polydispersities [30]. As a result, the monodisperse $S(q)$ works better in the low q region for high ϕ at low polydispersity. Even at intermediate ϕ, Eq. (8) tends to overpredict $S_{\mathrm{M}}(q)$ in the low q range, which leads to an underestimation of u for a SW system.

Furthermore, PY solution at high ϕ is known to overpredict the peak of $S(q)$. As a result the $S(q)$ needs to be calculated, using a reduced volume fraction ϕ' as given by the Verlet correction [27],

$$\phi' = \phi - \phi^2/16. \tag{9}$$

When the particles become sufficiently attractive, they form clusters which give rise to an excess scattering at low q. This additional scattering can be described by a Lorentzian term $S_c(q)$ corresponding to the structure factor of the colloidal clusters [31],

$$S_c(q) = \frac{I_M}{(1 + q^2\xi^2)^p}, \tag{10}$$

where I_M and ξ are proportional to the average mass and characteristic size of the clusters, and p is a power-law exponent related to the fractal morphology of the clusters. The exponent $p \sim d_f/2$, where d_f is the fractal dimension of the clusters.

The total intensity in the decoupling approximation including the cluster term is given by

$$I(q) = N_p \Delta\rho^2 V_p^2 \langle P(q)\rangle [S_{\mathrm{M}}(q) + S_c(q)]. \tag{11}$$

In the analysis of the low and the intermediate ϕ range Eq. (11) will be used. At very high ϕ, the cluster contribution is not apparent over the measured q range and the corresponding $I(q)$ will be analyzed using Eq. (1) with a polydisperse $P(q)$.

B. Dynamics

The dynamic light or x-ray scattering experiment provides the normalized time-averaged intensity auto-correlation function, $g_T^{(2)}(q,t)$ [32]. The quantity of interest is the intermediate scattering function, $f(q,t)$, obtained from the ensemble-averaged auto-correlation function, $g_E^{(2)}(q,t)$, which is related to the dynamic structure factor $S(q,t)$.

For an ergodic medium, time and ensemble averages are equivalent, $g_T^{(2)}(q,t) = g_E^{(2)}(q,t)$ [33,34], and $f(q,t)$ is calculated from the measured $g_T^{(2)}(q,t)$ [33,35],

$$g_T^{(2)}(q,t) = 1 + g_T^{(2)}(q,0)[f(q,t)]^2. \tag{12}$$

For a purely diffusive system, $f(q,t)$ at short times decays by an exponential function

$$f(q,t) \sim \exp(-D_s q^2 t), \tag{13}$$

where D_s is the short-time diffusion constant and the corresponding relaxation time $\tau_c = 1/(D_s q^2)$. In the case of attractive particles, when their motion is constrained due to stickiness, the corresponding $f(q,t)$ decays by a stretched exponential function [36–38],

$$f(q,t) \propto \exp[-(t/\tau_s)^\beta], \tag{14}$$

where β is the stretching exponent, τ_s is related to τ_c by $\tau_c = \Gamma(1/\beta)(\tau_s/\beta)$, and Γ is the usual gamma function [25].

In the extreme case when the system becomes nonergodic, i.e., the particle diffusion is blocked either by the cages formed by the neighboring particles (repulsive glass) or by the stickiness (attractive glass), the measured $g_T^{(2)}(q,t)$ at a particular angle varies strongly when scanning through different positions in the sample. In this case, $f(q,t)$ can be extracted by two different methods. The former involves determining the ensemble averages by summing $g_T^{(2)}(q,t)$ over a large number of sample positions. In the latter approach, $f(q,t)$ is calculated from a single $g_T^{(2)}(q,t)$ and the corresponding time-averaged intensity $\langle I(q)\rangle_T$ at a particular position in the sample, together with $I(q)$ measurements averaged over many positions in the sample $\langle I(q)\rangle_E$ [33,35],

$$f(q,t) = 1 + \frac{\langle I(q)\rangle_T}{\langle I(q)\rangle_E}[\sqrt{1 + g_T^{(2)}(q,t) - g_T^{(2)}(q,0)} - 1]. \tag{15}$$

In this study, the latter approach is used to obtain $f(q,t)$.

For a nonergodic system, $f(q,t)$ decays to a finite value, $f(q,\infty)$, which is called the nonergodicity parameter [7]. $f(q,\infty)$ represents the frozen component of the fluctuations [34],

$$f(q,\infty) = 1 + \frac{\langle I(q)\rangle_T}{\langle I(q)\rangle_E}[\sqrt{2 - g_T^{(2)}(q,0)} - 1]. \tag{16}$$

As a result, $f(q,t)$ is a very sensitive quantity to differentiate between fluid, repulsive, and attractive glassy states.

C. Rheology

The rheology is a very powerful technique to distinguish between fluid, gel, and glassy states, provided the appropriate linear viscoelastic range is selected. The low-frequency elastic and loss moduli, G' and G'', respectively, show power-law dependence on angular frequency ω [39],

$$G' \sim \begin{cases} \omega^2 & \text{for } x > 3 \\ \omega^{x-1} & \text{for } 1 < x < 3 \end{cases}, \tag{17}$$

$$G'' \sim \begin{cases} \omega & \text{for } x > 2 \\ \omega^{x-1} & \text{for } 1 < x < 2 \end{cases}. \tag{18}$$

The transition from fluid to glass is characterized by a mean-

field *noise temperature* x that is equal to 1 at the glass transition, higher than 1 for fluidlike behavior, and lower than 1 in the glassy state. At the glass transition both moduli become nearly frequency independent [39–42].

III. EXPERIMENTAL TECHNIQUES

The USAXS measurements were performed at the High Brilliance beamline (ID2) at the European Synchrotron Radiation Facility (ESRF) in Grenoble, France using a Bonse-Hart instrument [43]. This setup involved two crossed analyzers which permitted us to obtain intensity profiles, $I(q)$, directly in an absolute scale without any smearing. The intensity was recorded with a high dynamic range avalanche photodiode. Typical USAXS scans provided a useful q range of 10^{-3} nm$^{-1} < q < 0.2$ nm^{-1}. The incident wavelength (λ_0) and intensity were 1 Å and 5×10^{12} photons/s, respectively. For $q < 6 \times 10^{-2}$ nm^{-1} the beam intensity was attenuated by more than 15 times. Optionally, the coherent part of the beam was selected with a small slit setting (0.03×0.03 mm) and the scattered signal was fed to an ALV 5000-E dual channel correlator. This allowed us to record simultaneously the intensity-intensity autocorrelation function $g_T^{(2)}(q,t)$. Supplementary SAXS measurements were made using the 10 m pinhole SAXS camera at ID2, covering the q range 0.01 nm$^{-1} < q < 0.5$ nm^{-1}. The measured two-dimensional (2D) patterns were normalized to an absolute scale and azimuthally averaged to obtain the $I(q)$. Additional DXS (x-ray photon correlation spectroscopy) measurements were performed at the Troïka beamline (ID10A, ESRF), which is optimized for coherent scattering experiments [44]. In this case, the coherent beam was defined by a 12 μm pinhole, which gave a flux of 10^9 photons/s and the intensity was recorded using a scintillator detector coupled to an ALV 5000-E correlator. The incident wavelength was 1.6 Å in that setup. To limit radiation damage and beam heating, the sample was translated (avoiding continuous exposure at the same position) in between the measurements in both USAXS and DXS experiments. Possible multiple scattering in the USAXS region was checked by comparing the width of the rocking curve.

DLS experiments were carried out using a ALV goniometer fitted with a toluene bath. The incident laser wavelength was 532 nm (30 mW, diode pumped, frequency doubled Nd-YAG laser, Melles-Griot). The scattered intensity was recorded with an avalanche photodiode. The correlator was the same as that used in the DXS experiments. Only the measurements done at an angle of 90° are reported here. The acquisition time (t_a) of each $g_T^{(2)}(q,t)$ was 600 s. The ensemble-averaged intensity was estimated by rotating the sample.

Samples for USAXS and DXS were contained in thin-walled flat borsilicate glass capillaries with sample thickness 0.5 or 1.0 mm for dilute samples. The capillaries were flame sealed to avoid evaporation loss. The form factor was measured using an in-vacuum flow-through capillary cell which reduced the background scattering and allowed to subtract the remaining background precisely. DLS samples were contained in cylindrical borsilicate capillaries of a diameter of 1.3 mm. The refractive indices of particles and solvent are 1.45 and 1.43, respectively. Under these conditions, the DLS measurements do not suffer significantly from multiple scattering. Supplementary USAXS experiments were performed on the same samples used in DLS. This permitted us to determine the $S(q)$ and ϕ by USAXS.

For USAXS and DXS the sample was placed in a thermostated oven with temperature stability better than ±0.005 °C. For DLS, the temperature of the toluene bath was regulated within 0.2 °C using an external water bath (Huber). Prior to measurements, samples were homogenized at the high temperature fluid state.

High resolution rheology was performed using a stress-controlled rheometer (Haake, RS300 with microtorque option) with plate-plate geometry thermostated to ±0.01 °C. Typical sample diameter and thickness were 8 and 0.5 mm, respectively. The gap was varied to check the influence on the measurement. Special care was exercised for reducing the evaporation losses using a solvent trap and correcting for the real size of sample between the plates. However, the maximum duration of the experiment was still limited to less than 24 h. The applied low-frequency oscillatory stress was well within the linear viscoelastic range which was verified by a stress sweep at each temperature for several ω values. In addition, the sinusoidal form of the response signal was checked for each measurement. After the experiment, the sample was extracted and ϕ was determined by USAXS.

IV. MATERIALS

The silica particles were prepared using the Stöber method [45] and subsequently grafted with stearyl alcohol (1-octadecanol) using the well-known procedure [46]. The particles were stored in cyclohexane where they remain stable for years.

The required amount of samples were prepared by evaporating the cyclohexane and resuspending in n-dodecane (Sigma-Aldrich, 99%) in a clean glass vial. In order to remove possible permanent aggregates, the original suspension in cyclohexane was filtered through millipore filters (0.4 microns). After the addition of the required amount of dodecane, the vial was heated to 60 °C and agitated in an ultrasonic bath for more than 20 min. The samples for x-ray and light scattering measurements were transferred to the scattering cells at higher temperature (above 60 °C) where the particles form a stable suspension. For the concentrated samples, the hot suspension was aspirated into an open capillary using a gas-tight syringe (Hamilton) and then flame-sealed on both ends. In order to determine the scattering length density of the particles, a dilute suspension ($\phi < 0.01$) was prepared in chloroform. The contrast was varied by diluting the stock solution with cyclohexane. In order to account for the volume of mixing in binary solvent mixtures used for the contrast variation experiment, the density of each mixture was determined by an ANTON PAAR DMA 58 density meter. Both chloroform and cyclohexane are good solvents for the stearyl chains.

For the rheology experiments, the suspension was homogenized at 60 °C in the glass vial and then transferred onto the

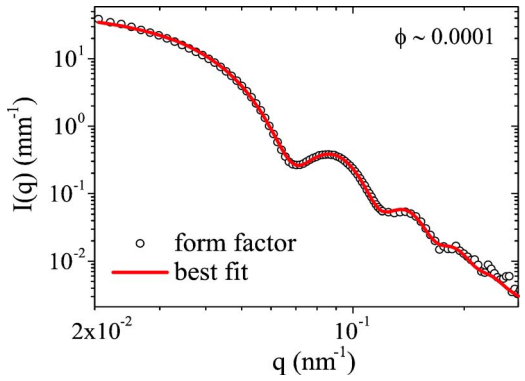

FIG. 2. (Color online) An experimental form factor of stearyl silica particles determined from a very dilute suspension ($\phi \sim 0.0001$) in dodecane at 50 °C. The solid line is a fit to the polydisperse sphere model with a Schulz size distribution with a mean radius 64.5 nm and polydispersity of 7.4%.

lower plate maintained at 18 °C (in order to avoid solvent evaporation) using a spatula. After the rheological experiment, a portion of the sample was extracted into flat x-ray capillaries for the determination of ϕ using USAXS.

V. RESULTS

A. Particle characterization

Figure 2 shows the $I(q)$ of a dilute sample in dodecane at 50 °C ($\phi \sim 0.0001$) obtained by SAXS. The continuous line is a fit to the polydisperse sphere model. The polydispersity is described by a Schulz size distribution with a mean particle radius $\bar{R}=64.5\pm0.1$ nm and polydispersity of $7.4\pm0.5\%$. However, $\bar{R}$ and polydispersity can vary between different batches of sample preparation by a couple of nanometers and a few percent, respectively. Therefore, they were reassessed for each sample using the high q oscillations in the scattered intensity.

To determine the scattering length density of the particles (ρ_p), a contrast variation experiment was performed. The initial sample in chloroform ($\phi < 0.01$) was systematically diluted with cyclohexane, thereby increasing ρ_p. All samples were contained in 2 mm capillaries and the measurements were performed at room temperature. Figure 3(a) shows the plot of ρ_p vs the square root of $I(0)$ derived from USAXS normalized by the corresponding ϕ. In this case the exact contrast match point was not reached but the contrast of the particles was estimated by extrapolating to zero intensity leading to $\rho_p \approx 0.00168$ nm^{-2} which corresponds to a silica density of 1.98×10^3 kg/m^3. This value is smaller than the known bulk density of amorphous silica (2.2×10^3 kg/m^3) but significantly higher than that found for Stöber silica particles (1.6×10^3–1.8×10^3 kg/m^3) [25,46]. This difference in densities may be attributed to the densification of the particles during the esterification process. For all subsequent analysis the measured value of ρ_p was used.

The exact concentration of colloids is often subject to uncertainties. The widely used method of measuring the concentration by solvent evaporation and dry weighing is susceptible to errors due to incomplete drying and the small amount of residuals to be weighed. Further complications arise when particles are porous and a complete evaporation could only be obtained by baking in a high vacuum. In the case of hard-sphere suspensions, the freezing concentration has been used to determine ϕ [1]. However, the exact agreement between theoretical freezing ϕ and experimental value has been assumed in this case. To overcome these uncertainties, the absolute scattered intensity together with the measured ρ_p was utilized [Eq. (1)] for determining ϕ *in situ*.

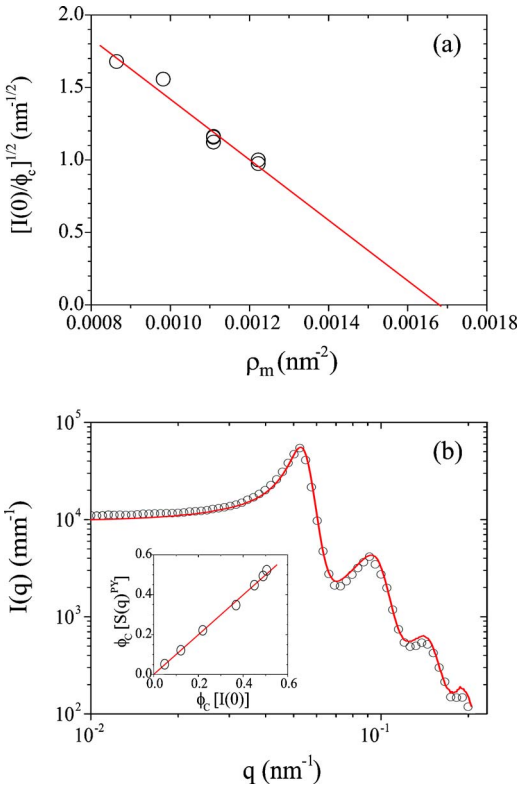

FIG. 3. (Color online) (a) The contrast variation of stearyl silica particles using a binary mixture solvent composed of cyclohexane and chloroform ($\phi < 0.01$). The linear fit to the data is extrapolated to the match point (0.00168 nm^{-2}) corresponding to a silica density of 1.98×10^3 kg/m^3. (b) The normalized USAXS intensity for a stearyl silica sample of $\phi \approx 0.5$ in dodecane at 60 °C. The continuous line corresponds to Eq. (1) with N_p constrained to the same value in both the prefactor and $S(q)$. The inset shows the comparison of the ϕ values determined from the absolute intensities $[I(0)]$ and the polydisperse $S(q)^{\mathrm{PY}}$.

Figure 3(b) shows the normalized USAXS intensity for a sample of stearyl silica spheres in dodecane with $\phi \approx 0.5$ at 60 °C. The continuous line corresponds to Eq. (1) with a hard-sphere $S(q)$. In this analysis, N_p is constrained to the same value in both the prefactor and ϕ in $S(q)$ [Eq. (3)]. The good agreement demonstrates that N_p can be reliably deduced from the absolute level of $I(q)$ for a hard-sphere system. The inset shows the comparison of the ϕ values determined from the absolute intensities $[I(0)]$ and the polydisperse $S(q)^{\mathrm{PY}}$ when they are allowed to vary independently. The linear behavior confirms the self-consistency in determining ϕ from absolute intensity. In the case of stearyl

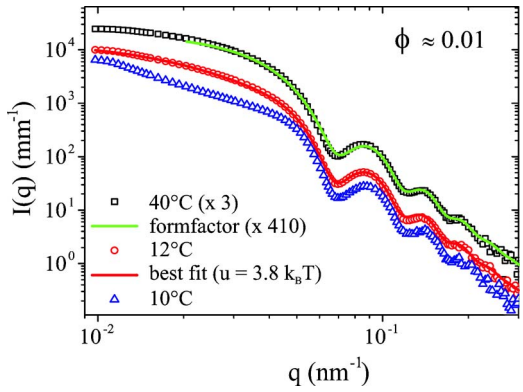

FIG. 4. (Color online) The SAXS curves showing the thermally reversible transition from repulsive to attractive particles in a dilute sample. At 40 °C the particles are repulsive and the shape of the scattering curve is nearly identical to the form factor. For comparison, the form factor data in Fig. 2 is also displayed after multiplying by a factor 410. The particles are attractive at 12 °C and the continuous line is a fit to Eq. (1) using the square-well $S(q)$ with $\epsilon=0.015$ and $u=3.8k_BT$, corresponding to $\tau_B \approx 0.12$. The scattering curve at 10 °C depicts the formation of aggregates and their sedimentation with time. Note that the upper curve (40 °C) is multiplied by 3 for clarity.

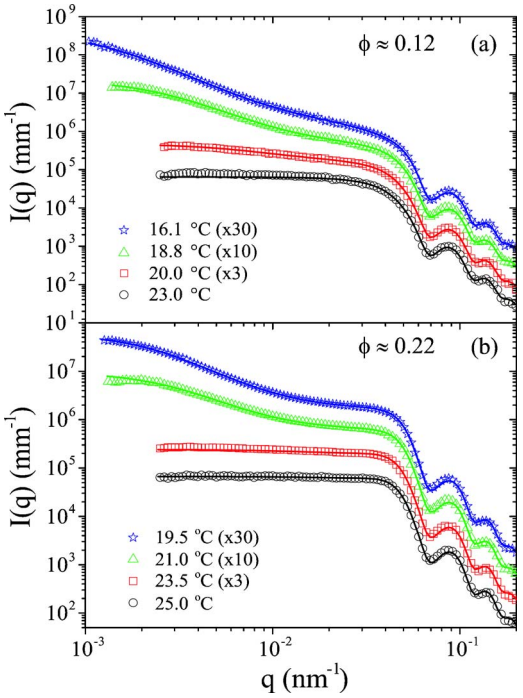

FIG. 5. (Color online) Representative USAXS curves and corresponding fits to Eq. (11) (continuous lines) for samples at intermediate volume fractions [(a) $\phi \approx 0.12$ and (b) $\phi \approx 0.22$]. The presented data demonstrate the onset of short-ranged attraction and the subsequent formation of colloidal clusters upon cooling the samples below T_A. For better visibility, the absolute $I(q)$ is multiplied by the factor indicated in the legend.

silica particles in dodecane, the contrast of the shell is matched with the solvent. Therefore the absolute intensity is essentially determined by the core volume fraction ϕ_C while $S(q)$ is influenced by the core as well as the nonoverlapping part of the shell. The agreement between the ϕ_C deduced from the absolute level of $I(q)$ and ϕ obtained from $S(q)$ fit [inset of Fig. 3(b)] suggests that the nonoverlapping region of the shell is smaller than 1 nm.

B. Microstructure and dynamics

Figure 4 illustrates the transition from repulsive to attractive particles for a dilute sample in dodecane ($\phi \approx 0.01$). At this ϕ range, the shape of the scattering curve at high temperature is nearly identical to the form factor except in the intensity level due to the difference in N_p. The transition to attractive spheres occurs at about $T_A \sim 15$ °C for this sample. However, the exact value of T_A can vary from sample to sample for the same ϕ by several degrees which could be attributed to the differences in the unremovable amount of cyclohexane or any other remnant solvent present in the sample. Another sensitive parameter that could affect T_A is the grafting density of the stearyl chains. In Fig. 4, the fitted line for $I(q)$ below T_A represents Eq. (1) involving $S(q)$ of the square-well potential with $u=3.6k_BT$ and $\epsilon=0.015$, corresponding to $\tau_B \approx 0.12$. This establishes the short-ranged nature of attraction in this system. The curve at 10 °C shows the formation of aggregates and their sedimentation with time, as indicated by the upturn of $I(q)$ at small q and the overall lowering of the curve. It should be noted that the $S(q)$ at this concentration range can also be described by a potential with a larger width ($\epsilon=0.1$) and a smaller value of u. As will be explained later, such a large value of ϵ is not consistent with the behavior of $S(q)$ at high ϕ.

In this system, the range of the SW potential is determined by the maximum overlap range of the stearyl layer [47,48]. The thickness of the stearyl layer is about 1.9 nm, as observed by SAXS at high q range using a concentrated sample (shell scattering from the coating). The above value of $\epsilon=0.015$ corresponds to Δ approximately equal to the thickness of the stearyl layer as given by Eq. (6), indicating a nearly complete overlapping of the stearyl chains. The transformation of stearyl silica particles from hard sphere to sticky hard sphere in certain organic solvents with temperature is usually attributed to the change of solvent quality near the θ temperature of the grafted chains [4]. The situation is rather different in the case of alkanes [47]. In bulk solutions, stearyl alcohol (octadecanol) precipitates from dodecane at these temperatures and eventually crystallizes. Therefore, the most likely scenario is a lyotropic ordering transition of the grafted stearyl chains at the surface of the particles [47,48]. However, there was no evidence for freezing of the solvent around the grafted chains from the wide angle x-ray scattering in contrast to that suggested by previous work [48]. It is unlikely that the macroscopic London–van der Waals attraction between silica cores changed so dramatically over such a small temperature range [49].

As the concentration is increased, similar behavior, shown in Fig. 4, can be observed when the attractive interaction is turned on by cooling the sample below T_A. Figure 5(a) shows the evolution of $I(q)$ for a sample of $\phi \approx 0.12$. In addition to the short-ranged attraction, there is a significant excess scat-

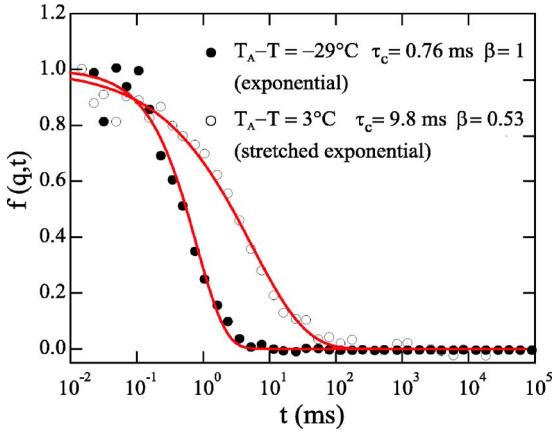

FIG. 6. (Color online) The intermediate scattering function obtained from DXS at $q=0.0173$ nm^{-1} for a sample with $\phi\approx 0.19$. The functional form changes from single to stretched exponential behavior when the particles become attractive.

tering at low q which can be attributed to the formation of clusters below T_A. This cluster scattering is described by the additional term in the structure factor given in Eq. (11). The exponent, p is found to be 1.15 which suggests that the clusters have fractal morphology with $d_f\approx 2.3$. This is similar to the value of d_f observed in a closely related system [50,51], but significantly different from Porod behavior ($p=2$) observed in certain other short-ranged attractive systems [23,41].

Figure 5(b) shows the corresponding behavior at a higher $\phi\approx 0.22$. As in the previous figure $I(q)$ is adequately described by Eq. (11). The differences between the fit parameters for these two samples will be discussed later. In order to better understand the observed static behavior, the dynamics of the system in this concentration range was probed using DXS. Figure 6 shows representative intermediate scattering functions for a sample $\phi\approx 0.19$, obtained from $g_T^{(2)}(q,t)$. The decay of $f(q,t)$ changed from single to stretched exponential as the temperature is decreased below T_A, implying constrained dynamics with a large value of τ_c. The details of the system at the intermediate range can be better illustrated by comparing the attractive well parameters together with τ_c.

Figure 7 shows the evolution of the fit parameters for the data presented in Fig. 5(a) (initial $\phi\approx 0.12$). As the temperature is decreased, the attractive well evolves together with a slowing down of the dynamics. Concurrently, there is an increase in the local ϕ which can be attributed to the clustering process. When the volume fraction within the clusters reaches a certain value, the relaxation rate $1/\tau_c$ goes to zero, indicating the complete jamming of the local dynamics. The arrested dynamics prevents a macroscopic phase separation of the system. For a comparison, Fig. 8 presents the evolution of the fit parameters for the data shown in Fig. 5(b) (initial $\phi\approx 0.22$). At this concentration, the local ϕ remains the same within the uncertainties of the fit. However, $1/\tau_c$ goes to zero as the depth of the potential reaches about k_BT. In this ϕ range, the deduced value of u is somewhat lower than that in Fig. 4. For instance τ_B has reached only 0.8 at 16.1 °C in Fig. 5(a). This could be attributed to a cumulative

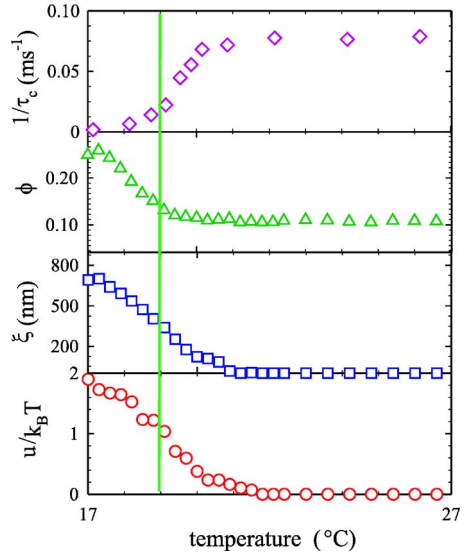

FIG. 7. (Color online) The evolution of the fit parameters for the data shown in Fig. 5(a) and the corresponding relaxation rates deduced from DXS at $q=6.3\times 10^{-3}$ nm^{-1}. The vertical line is a guide to the eye, indicating the temperature at which the fitted $u\approx k_BT$.

effect of the decoupling approximation and the correlation of the cluster term with the attractive part of $S(q)$.

When the concentration is increased further, the cluster scattering became less evident in the USAXS region. Figure 9 shows the typical variation of $I(q)$ in the low q region. The dominant effect is the evolution of interaction (u increasing to $2k_BT$, corresponding to $\tau_B\sim 0.75$ at 29 °C). In addition, the cluster term is necessary to fully describe the total $I(q)$. At this concentration range, the decoupling approximation breaks down [overestimation of $S(q)$ at low q] and, therefore, the fitting was performed using a monodisperse $S(q)$ in Eq. (11).

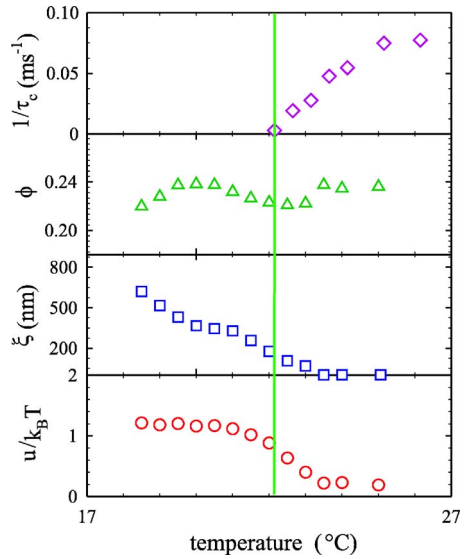

FIG. 8. (Color online) The evolution of the fit parameters for the data shown in Fig. 5(b) and the corresponding relaxation rates deduced from DXS at $q=6.3\times 10^{-3}$ nm^{-1}. The vertical line is a guide to the eye, indicating the temperature at which the fitted $u\approx k_BT$.

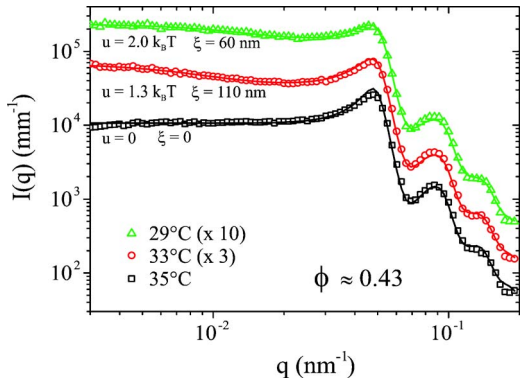

FIG. 9. (Color online) The USAXS curves and corresponding fits (continuous lines) for a sample at higher $\phi \approx 0.43$ showing the typical evolution of $S(q)$. The fit parameters for u and ξ are indicated in the legend, and $\tau_B \approx 0.75$ at 29 °C. For better visibility, the absolute $I(q)$ is multiplied by the factor indicated.

The clustering effect became less apparent at still higher concentrations. Figure 10(a) shows the evolution of the intensity for a sample of $\phi \approx 0.535$. The low q upturn in $I(q)$ observed at intermediate ϕ range has changed to a plateau region. Figure 10(b) depicts the corresponding change in $S(q)$, fitted with the SW term alone [Eq. (1)]. At this concentration range, the Verlet correction became more important and therefore the PY solution used the reduced ϕ given by

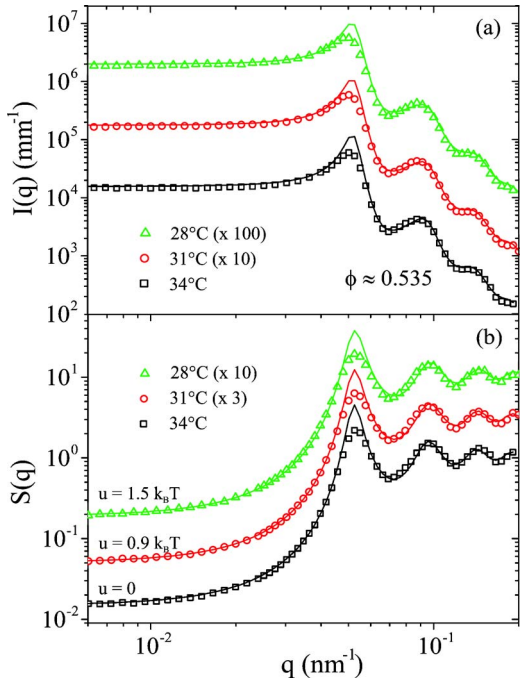

FIG. 10. (Color online) (a) The evolution of $I(q)$ at high $\phi \approx 0.535$ showing only subtle variations in $S(q)$. The data can be satisfactorily fitted by the square-well model without the cluster term (Eq. 1, continuous lines). (b) $S(q)$ deduced from above $I(q)$ and the corresponding fit to the square-well model (continuous lines) with the indicated u and $\epsilon = 0.015$ values ($\tau_B \approx 1.24$ at 28 °C). The mismatch at the peak of $S(q)$ is attributed to the effect of the polydispersity. For better visibility, $I(q)$ and $S(q)$ are multiplied by the factor indicated in the legend.

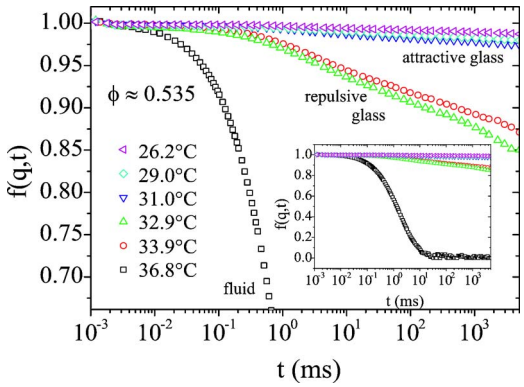

FIG. 11. (Color online) The intermediate scattering function obtained from DLS at $q = 0.024$ nm^{-1} for the same sample as in Fig. 10 ($\phi \approx 0.535$). At high temperature, the sample behaves fluidlike as indicated by the exponential decay of $f(q,t)$ (see also the inset). The systematic slowing down of the dynamics upon cooling indicates the transition to repulsive glass [$f(q,\infty) \approx 0.7$] and then to attractive glass [$f(q,\infty) \approx 0.98$].

Eq. (9). The mismatch near the main peak of $S(q)$ is attributed to the effect of polydispersity [27] and also the possible overprediction of the series expansion of PY [29]. At this ϕ, the maximum observed value of the potential depth reaches about $1.5k_BT$ ($\tau_B \sim 1.24$). The significance of Eqs. (3) and (7) is more acutely felt as indicated by a small decrease of $\sigma \sim 1-2$ nm from the hard-sphere value (134 nm) when the system transforms from repulsive to attractive spheres. As a result, the increase of the effective ϕ due to square-well attraction [Eq. (7)] is compensated by this decrease of σ. Therefore the fits used a constant value of ϕ over this concentration range. Furthermore, the insignificant shift in the q value of $S(q)$ peak with the onset of attraction indicates that ϵ has a small range (=0.015) in this system. This feature of $S(q)$ is somewhat different from the light scattering results on reentrant systems involving colloid-polymer mixtures [16,18]. The main difference in this case is that USAXS data provided the true partial $S(q)$ of colloid-colloid interactions and there is no cross term involved unlike in colloid-polymer mixtures. In addition, $S(q)$ is properly normalized, using an experimentally determined $P(q)$ and the high q limit of $I(q)$ [$S(q) \approx 1$].

Although the observed variation of $S(q)$ is somewhat subtle at this ϕ, the dynamics is expected to evolve significantly [42,52]. Figure 11 shows the dramatic slowing down of the dynamics as probed by DLS. At high temperature, the sample behaved like a fluid as indicated by the exponential decay of $f(q,t)$ (see the inset of Fig. 11). When the temperature is decreased, $f(q,t)$ changed to nonergodic behavior [$f(q,\infty) \approx 0.7$] prior to the evolution of SW [$u=0$ in Fig. 10(b)]. In addition, $f(q,t)$ tends to show the double relaxation characteristic of a repulsive glass transition. These two decays correspond to α and β processes (breakup and rattling of cages, respectively) [13,38]. With further lowering of temperature, the system transforms to attractive spheres as shown in Fig. 10(b). In the attractive state, $f(q,t)$ remained flat with [$f(q,\infty) \approx 0.98$] corresponding to almost completely jammed dynamics. This means that the system trans-

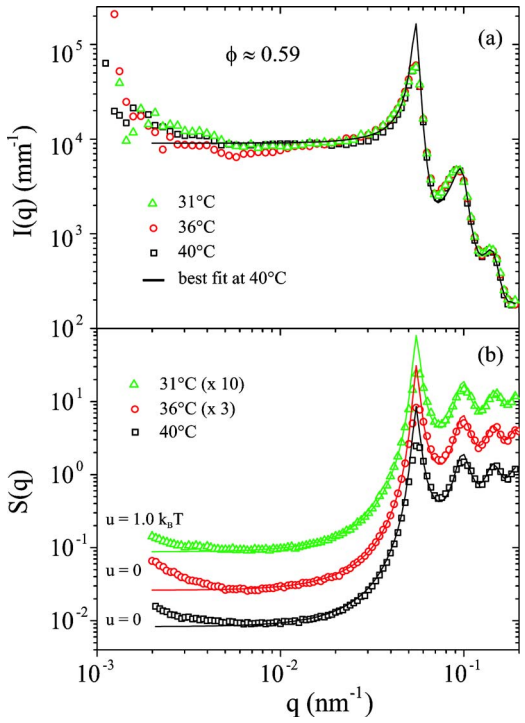

FIG. 12. (Color online) (a) The evolution of $I(q)$ at higher $\phi \approx 0.59$ demonstrating little changes in static structure with temperature. The fitted line at 40 °C refers to hard-sphere $S(q)$ [Eq. (1)]. (b) $S(q)$ derived from the data in (a) and the respective fits to the square-well model (continuous lines). For better visibility, the absolute $S(q)$ is multiplied by the factor indicated in the legend.

formed from repulsive to attractive glass with the introduction of short-ranged attraction [see also Fig. 10(b)].

Analogous behavior was observed at still higher concentration. Figure 12 ($\phi \approx 0.59$) shows that the changes in static structure is barely detectable. In the glassy states $S(q)$ tends to show a low q upturn, presumably due to heterogeneities in the sample [53]. Although the variations were subtle, the change can be described by the evolution of the square-well potential as for $\phi \approx 0.535$. Figure 13 shows the corresponding dynamics over this temperature range. In this case, the high temperature fluid phase is not accessible within the range of the toluene bath used in the experiment (<70 °C). As in the previous case, the double relaxation can be clearly seen in the repulsive state with $f(q,\infty) \approx 0.7$ at 36 °C. The $f(q,t)$ becomes flat in the attractive state with $f(q,\infty) \approx 0.99$ at 24 °C. In the intervening region demarcating the repulsive and attractive glassy states, $f(q,t)$ shows very pronounced oscillations at longer t (reminiscent of an heterodyning effect). These oscillations presumably induced by external mechanical vibrations can be described by a function, $f(q,t) \sim \cos(\omega_s t)$, as presented in the inset (with $\omega_s = 0.345$ rad/s). This peculiar behavior is suggestive of the slow speed ($=\omega_s/q$) and low damping of acoustic waves in the sample at this particular dynamical state.

Finally, the error bars in the fit parameters of static structure are smaller than the size of the symbols in the plots except in the transition region below T_A. In this range, a competition between the attractive and the cluster terms be-

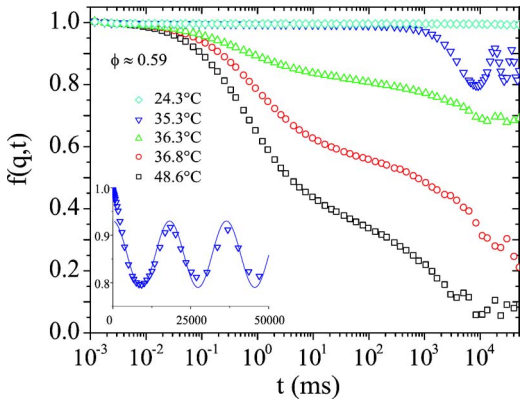

FIG. 13. (Color online) The intermediate scattering function obtained from DLS at $q=0.024$ nm^{-1} for the same sample as in Fig. 12 ($\phi \approx 0.59$). The high temperature fluid phase is not accessible within the experimental temperature range (<70 °C) and the sample remains in the repulsive glass state above 36 °C [$f(q,\infty) = 0.7$]. With further cooling, the sample transforms into an attractive glass below 33 °C. In the intervening temperature range, $f(q,t)$ shows pronounced oscillations at longer t, suggesting very slow propagation and damping of mechanical vibrations. The inset shows a smooth cosine behavior of these oscillations, $\cos(\omega_s t)$, with $\omega_s = 0.345$ rad/s at 35.3 °C. $f(q,\infty)$ reaches nearly 1 below 25 °C, indicating a completely jammed state.

comes evident. As a result, the uncertainties in the fit parameters can be as high as ±25%. Nevertheless, the terminal values of the parameters have a very small uncertainty. The error bars of $f(q,t)$ depend on the particular choice of sample position (and the angle). The errors originate mainly from finite acquisition time (t_a) for each time averaged $g_T^{(2)}(q,t)$, and the variance in measured time and ensemble-averaged intensities [34,54]. The estimated uncertainty is of the order of $(\tau_c/t_a)^{0.5}$. $f(q,t)$ was calculated from different $\langle g_T^{(2)}(q,t)\rangle$ and the variation between different runs is less than 8%. The reported $f(q,t)$ is an average over several measurements.

C. Rheology

The observed features in the dynamics can be complemented by bulk rheology. Figure 14(a) depicts a dramatic variation of G' and G'' as a function of the temperature for an applied stress of 5 Pa with $\omega = 0.628$ rad/s. The attractive to repulsive transition is characterized by a significant decrease of G' and G''. Figure 14(b) depicts the frequency dependence of G' and G'' at selected temperatures. Over this temperature range, G' and G'' showed only very weak frequency dependence ($\sim \omega^{x-1}, x \to 1$) demonstrating the glassy behavior at all temperatures investigated [see Eqs. (17) and (18)]. Figure 15(a) illustrates the onset of flow as a function of applied stress at two different temperatures. At this ϕ the system transforms from attractive glass to fluid as the temperature is increased [55]. Figure 15(a) illustrates that the yield stress decreases as the attractive glass-fluid transition is reached. In Fig. 15(a), the yield stress corresponds to the point where the measured strain rises or G' drops sharply with the applied stress. Furthermore, the attractive and repul-

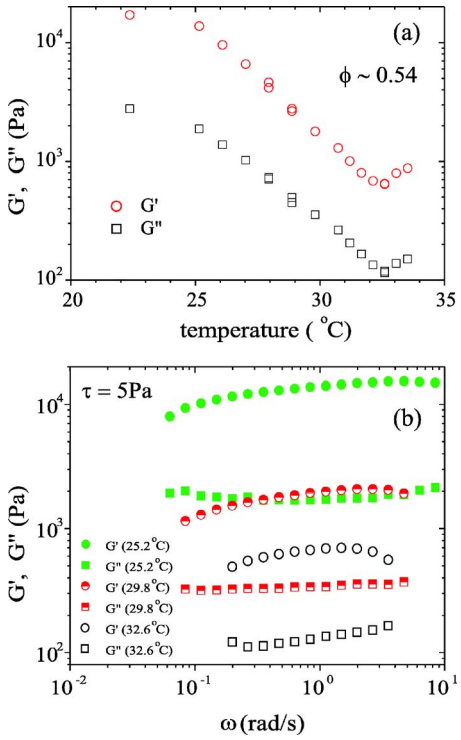

FIG. 14. (Color online) (a) The variation of low frequency elastic moduli as a function of temperature for an applied stress of 5 Pa and ω=0.628 rad/s ($\phi \sim 0.54$). The dramatic change in the particle dynamics is manifested by a significant increase in the elastic moduli G' and G'' as the temperature is lowered. (b) The weak frequency dependence of G' and G'' depicts the glassy nature of the sample at selected temperatures.

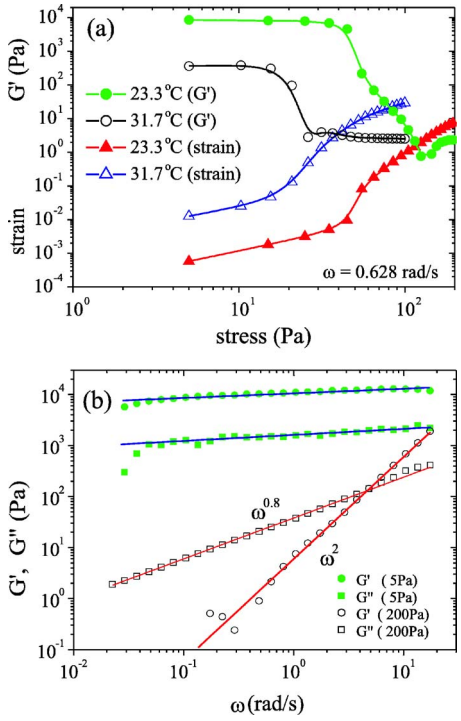

FIG. 15. (Color online) (a) The variation of G' and strain with applied stress for a sample of $\phi \sim 0.52$ at two temperatures, illustrating the limiting linear viscoelastic range (ω=0.628 rad/s). (b) Frequency dependence of G' and G'' at low and high stress values (5 and 200 Pa, respectively) showing glassy and fluid behavior as functions of the applied stress for the same sample of $\phi \sim 0.52$ in the attractive glassy state (23.3 °C).

sive glasses can be transformed to fluidlike behavior by applying a higher stress. Figure 15(b) shows the glassy and fluidlike behavior for $\phi \sim 0.52$ at 23.3 °C at two different stress values. The refluidization ($G' \sim \omega^2, G'' \sim \omega$) of the system at the higher stress value (200 Pa) is consistent with the generalized jamming phase diagram for an attractive system [56].

The main uncertainty for G' and G'' arise from the aging behavior of the sample. The presented G' and G'' correspond to their values after reaching the plateau level at each temperature step. In addition, the measurement time and ω range were restricted to an interval over which G' and G'' remained nearly constant. In the linear viscoelastic domain at low stress levels, G' and G'' are not sensitive to the applied stress. In the repulsive state as the sample is heated above 35 °C, G' and G'' tend to marginally increase which could be attributed to slight solvent evaporation. At intermediate ϕ between 0.52 and 0.536, reentrantlike behavior can be observed as the sample is heated from the attractive state. For instance G' first decreased sharply and then increased [a dip in G' more pronounced than in Fig. 14(a)]. However, this transition is also dependent on the temperature step and the magnitude of the applied stress. Therefore, the rheological characterization of the reentrant transition requires more precise scrutiny of linear viscoelastic range.

VI. DISCUSSION

The static structure, dynamics, and rheological behavior of a model short-ranged interacting colloidal system was studied over a wide concentration range including the vicinity of the reentrant glass-fluid-glass transition. The thermally reversible nature of the transition enabled the quantitative comparison of measured properties more straightforward. The different parameters involved in modeling were deduced by independent experiments. The short-ranged nature of the interparticle interaction was established from dilute samples. The intermediate concentration range allowed us to monitor the evolution of the square-well parameters and the formation of aggregates and their subsequent gelation. In this range, the macroscopic phase separation is presumably interrupted by the gelation [37]. Recent experiments using colloid-polymer mixtures reported a spinodal decomposition assisted gelation process [57]. However in this system, the location of spinodal line is expected to be at a much smaller value of τ_B ($\leqslant 0.1$) [3,5]. The high ϕ data showed only subtle changes in the static structure but the highly quantitative measurements allowed us to deduce the relevant changes in the SW parameters.

The complementary dynamic scattering experiments permitted us to probe the dramatic changes in the particle dynamics across the glass transitions and relate them to static properties. At low ϕ the dynamics changed from single ex-

ponential to stretched exponential behavior and the complete slowing down of the dynamics was only observed with enhanced packing within the clusters. Although the temperature is a very convenient parameter to tune the interactions, additional effects such as mentioned below might appear. For instance, there is a change in the macroscopic London–van der Waals interactions due to the temperature dependence of the dielectric constant [49]. In addition, the effective ϕ of colloids decreases slightly ($<0.02\%/^\circ\mathrm{C}$) as the temperature is increased due to the thermal expansion of the solvent. The latter effect marginally contributes to the transition from fluid to repulsive glass shown in Fig. 11. Alternatively, this transition could be indicative of the peculiar trajectory of the glass line B_1 in Fig. 1 in which the system transforms from repulsive glass to fluid behavior as τ_B is increased. Such a transition is also observed in a concentrated block copolymer system [17] and is reminiscent of the B_1 line obtained by MCT for a SW width of 4% [6].

The attractive and repulsive glasses demonstrate distinctly different behavior of the nonergodicity parameter. The attractive glass shows a very high amount of the frozen component $[f(q,\infty)\rightarrow 1]$. More interestingly at high volume fractions, the transition between attractive and repulsive glass is characterized by a peculiar dynamical state, involving an elastic glass as indicated by the slow propagation and low damping of mechanical vibrations. This behavior could be related to anomalies in the elastic properties near the third-order singular point (A_3).

Complementary rheological measurements confirmed two glassy states in this system and vividly demonstrated that the attractive glass has a higher rigidity and yield stress. The sharp attractive to repulsive transition is in agreement with the predictions of MCT [6,52] but differs from more recent numerical simulation which suggested that the activated bond breaking preempts a sharp glass-glass transition [58]. The aging times involved in experiments and simulations vary by many orders of magnitude which might explain the observed difference. The soft glassy rheology is sensitive to the applied stress. This is consistent with the generalized jamming phase diagram of an attractive system [56]. As a result, the experimental results presented here clearly relate the static and dynamic behavior predicted by MCT and the phenomenological approach based on jamming phase diagram.

Further dynamic scattering and rheological experiments will be useful to explore the dynamical singularities near the so-called A_3 point [59]. Finally, it is interesting to note that the observed ϕ corresponding to glass-fluid transition is close to the MCT value for a hard-sphere system (0.516) [6,13].

VII. CONCLUSION

The results obtained in this work clearly demonstrate a broad range of static and dynamic behavior as a function of ϕ for a square-well attractive system. At low and intermediate volume fractions, the static structure factor exhibits the features of phase separation and gelation, respectively. With the onset of attraction, the static structure factor shows only small variations at high volume fractions but the corresponding dynamics displays remarkable features, demonstrating the kinetic nature of the underlying transitions. From the long-time behavior of the intermediate scattering function, repulsive to attractive glass transition was identified. This was complemented by the behavior of the low frequency shear moduli obtained from bulk rheology. The observed features are in agreement with recent mode-coupling theoretical predictions [52], as well as the generalized jamming phase diagram of attractive colloidal systems [56], but the sharper glass-glass transition differs from computer simulations [58]. At high volume fraction, the static structure is similar to the repulsive glass, but the rheological parameters are closer to the attractive glass in both attractive and repulsive states.

The model system presented here is convenient for testing the theoretical predictions, as well as for quantitative scattering experiments. Ultrasmall-angle x-ray scattering is a powerful technique to elucidate the multilevel structural features in this type of systems. The volume fraction is often an uncertain parameter in colloid science. As shown here, the absolute scattered intensity can be used to deduce the volume fraction *in situ*. In addition, the combination with dynamic scattering allows us to obtain static interactions, dynamics, and phase behavior from the same experiment. These features can be further exploited to resolve certain longstanding issues in colloid science.

ACKNOWLEDGMENTS

We thank P. Panine, J. Gorini, and P. Bösecke for technical support. We also thank J. Vermant, B. Cabane, and A. R. Rennie for discussion. The European Synchrotron Radiation Facility is acknowledged for the financial support and the provision of synchrotron beam time.

[1] P. N. Pusey, in *Liquids, Freezing and Glass Transition*, edited by J. P. Hansen, D. Levesque, and J. Zinn-Justin (North-Holland, Amsterdam, 1991), p. 787.
[2] H. Löwen, Phys. Rep. **237**, 249 (1994).
[3] R. J. Baxter, J. Chem. Phys. **49**, 2770 (1968).
[4] H. Verduin and J. K. G. Dhont, J. Colloid Interface Sci. **172**, 425 (1995).
[5] S. V. G. Menon, C. Manohar, and K. S. Rao, J. Chem. Phys. **95**, 9186 (1991).
[6] K. Dawson, G. Foffi, M. Fuchs, W. Gotze, F. Sciortino, M. Sperl, P. Tartaglia, T. Voigtmann, and E. Zaccarelli, Phys. Rev. E **63**, 011401 (2000).
[7] J. Bergenholtz and M. Fuchs, Phys. Rev. E **59**, 5706 (1999).
[8] E. Zaccarelli, G. Foffi, K. A. Dawson, F. Sciortino, and P. Tartaglia, Phys. Rev. E **63**, 031501 (2001).
[9] F. Sciortino, P. Tartaglia, and E. Zaccarelli, Phys. Rev. Lett.

91, 268301 (2003).
[10] M. A. Miller and D. Frenkel, Phys. Rev. Lett. **90**, 135702 (2003).
[11] F. Sciortino, S. Mossa, E. Zaccarelli, and P. Tartaglia, Phys. Rev. Lett. **93**, 055701 (2004).
[12] K. Kroy, M. E. Cates, and W. C. K. Poon, Phys. Rev. Lett. **92**, 148302 (2004).
[13] F. Sciortino and P. Tartaglia, Adv. Phys. **54**, 471 (2005).
[14] E. Zaccarelli, G. Foffi, K. A. Dawson, S. V. Buldyrev, F. Sciortino, and P. Tartaglia, Phys. Rev. E **66**, 041402 (2002).
[15] G. Foffi, K. A. Dawson, S. V. Buldyrev, F. Sciortino, E. Zaccarelli, and P. Tartaglia, Phys. Rev. E **65**, 050802(R) (2002).
[16] T. Eckert and E. Bartsch, Phys. Rev. Lett. **89**, 125701 (2002).
[17] S.-H. Chen, W.-R. Chen, and F. Mallamace, Science **300**, 619 (2003); W.-R. Chen, F. Mallamace, C. J. Glinka, E. Fratini, and S.-H. Chen, Phys. Rev. E **68**, 041402 (2003).
[18] K. N. Pham, A. M. Puertas, J. Bergenholtz, S. U. Egelhaaf, A. Moussaïd, P. N. Pusey, A. B. Schofield, M. E. Cates, M. Fuchs, and W. C. K. Poon, Science **296**, 104 (2002); K. N. Pham, S. U. Egelhaaf, P. N. Pusey, and W. C. K. Poon, Phys. Rev. E **69**, 011503 (2004).
[19] M. Kapnistos, D. Vlassopoulos, G. Fytas, K. Mortensen, G. Fleischer, and J. Roovers, Phys. Rev. Lett. **85**, 4072 (2000).
[20] P. N. Segre, V. Prasad, A. B. Schofield, and D. A. Weitz, Phys. Rev. Lett. **86**, 6042 (2001).
[21] V. Trappe, V. Prasad, L. Cipelletti, P. N. Segre, and D. A. Weitz, Nature (London) **411**, 772 (2001).
[22] S. R. Bhatia and A. Mourchid, Langmuir **18**, 6469 (2002).
[23] D. Pontoni, T. Narayanan, J.-M. Petit, G. Grubel, and D. Beysens, Phys. Rev. Lett. **90**, 188301 (2003).
[24] J. Grandjean and A. Mourchid, Europhys. Lett. **65**, 712 (2004); Phys. Rev. E **72**, 041503 (2005).
[25] D. Pontoni, S. Finet, T. Narayanan, and A. R. Rennie, J. Chem. Phys. **119**, 6157 (2003).
[26] M. Kotlarchyk and S.-H. Chen, J. Chem. Phys. **79**, 2461 (1983).
[27] R. Klein and B. D'Aguanno, in *Light Scattering: Principles and Development*, edited by W. Brown (Clarendon Press, Oxford, 1996), p. 30.
[28] W.-R. Chen, S.-H. Chen, and F. Mallamace, Phys. Rev. E **66**, 021403 (2002).
[29] G. Foffi, E. Zaccarelli, F. Sciortino, P. Tartaglia, and K. A. Dawson, J. Stat. Phys. **100**, 363 (2000).
[30] E. W. Kaler, in *Modern Aspects of Small-Angle Scattering*, edited by H. Brumberger (Kluwer Academic, Dordrecht, 1995), p. 329.
[31] P. Schmidt, in *Modern Aspects of Small-Angle Scattering*, edited by H. Brumberger (Kluwer Academic, Dordrecht, 1995), p. 1.
[32] R. Pecora, *Dynamic Light Scattering. Applications of Photon Correlation Spectroscopy* (Plenum Press, New York, 1985).
[33] P. N. Pusey and W. Van Megen, Physica A **157**, 705 (1989).
[34] A. Moussaïd, P. N. Pusey, J. J. M. Slot, and J. G. H. Joosten, Macromolecules **32**, 3774 (1999).
[35] A. Moussaïd, S. J. Candau, and J. G. H. Joosten, Macromolecules **27**, 2102 (1994).
[36] A. H. Krall and D. A. Weitz, Phys. Rev. Lett. **80**, 778 (1998).
[37] E. Zaccarelli, I. Saika-Voivod, S. V. Buldyrev, A. J. Moreno, P. Tartaglia, and F. Sciortino, J. Chem. Phys. **124**, 124908 (2006).
[38] L. Cipelletti and L. Ramos, J. Phys.: Condens. Matter **17**, R253 (2005).
[39] P. Sollich, Phys. Rev. E **58**, 738 (1998).
[40] T. G. Mason and D. A. Weitz, Phys. Rev. Lett. **75**, 2770 (1995).
[41] S. Ramakrishnan, Y. L. Chen, K. S. Schweizer, and C. F. Zukoski, Phys. Rev. E **70**, 040401(R) (2004).
[42] F. Mallamace, P. Tartaglia, W.-R. Chen, A. Faraone, and S.-H. Chen, J. Phys.: Condens. Matter **16**, S4975 (2004).
[43] T. Narayanan, O. Diat, and P. Boesecke, Nucl. Instrum. Methods Phys. Res. A **467**, 1005 (2001).
[44] D. L. Abernathy, G. Grübel, S. Brauer, I. McNulty, G. A. Stephenson, S. G. J. Mochrie, A. R. Sandy, N. Mulders, and M. Sutton, J. Synchrotron Radiat. **5**, 37 (1998).
[45] W. Stöber, A. Fink, and E. Bohn, J. Colloid Interface Sci. **26**, 62 (1968).
[46] A. K. Van Helden and A. Vrij, J. Colloid Interface Sci. **76**, 418 (1980).
[47] C. G. de Kruif and J. A. Schouten, J. Chem. Phys. **92**, 6098 (1990).
[48] C. G. de Kruif and J. C. van Miltenburg, J. Chem. Phys. **93**, 6865 (1990).
[49] J. Edwards, D. H. Everett, T. Osullivan, I. Pangalou, and B. Vincent, J. Chem. Soc., Faraday Trans. 1 **80**, 2599 (1984).
[50] M. J. Solomon and P. Varadan, Phys. Rev. E **63**, 051402 (2001).
[51] H. Hoekstra, J. Mewis, T. Narayanan, and J. Vermant, Langmuir **21**, 11017 (2005).
[52] E. Zaccarelli, G. Foffi, K. A. Dawson, S. V. Buldyrev, F. Sciortino, and P. Tartaglia, Phys. Rev. E **66**, 041402 (2002).
[53] H. Weber, W. Paul, W. Kob, and K. Binder, Phys. Rev. Lett. **78**, 2136 (1997).
[54] K. Schätzel, Appl. Opt. **32**, 3880 (1993).
[55] T. Narayanan, M. Sztucki, G. Belina, and F. Pignon, Phys. Rev. Lett. **96**, 258301 (2006).
[56] A. Kumar and J. Wu, Appl. Phys. Lett. **84**, 4565 (2004).
[57] S. Manley, H. M. Wyss, K. Miyazaki, J. C. Conrad, V. Trappe, L. J. Kaufman, D. R. Reichman, and D. A. Weitz, Phys. Rev. Lett. **95**, 238302 (2005).
[58] E. Zaccarelli, G. Foffi, F. Sciortino, and P. Tartaglia, Phys. Rev. Lett. **91**, 108301 (2003).
[59] A. Lawlor, D. Reagan, G. D. McCullagh, P. De Gregorio, P. Tartaglia, and K. A. Dawson, Phys. Rev. Lett. **89**, 245503 (2002).